Secular Changes of Annual and Interannual Variability in the Tropics during the Past Century

DAIFANG GU AND S. G. H. PHILANDER

Program in Atmospheric and Oceanic Sciences, Princeton University, Princeton, New Jersey

(Manuscript received 13 October 1993, in final form 18 August 1994)

ABSTRACT

Wavelet transforms, which can unfold signals in both time and frequency domains, are used to analyze the Comprehensive Ocean and Atmospheric Data Sets for the period 1870–1988. The focus is on secular changes in the interannual variability and the annual cycle of selected equatorial regions. The amplitude of El Niño/Southern Oscillation (ENSO) is found to be large from 1885 to 1915, to be small during the period 1915–1950, and to increase rapidly after about 1960. Surprisingly, the decadal variations in the amplitude of ENSO are not matched by similar decadal variations in the amplitude of the annual cycle.

On short timescales of 2–5 years, ENSO strongly influences the annual cycle in certain parts of the central and eastern tropical Pacific where the thermocline is shallow. The annual cycle is weak in warm El Niño years and is strong in cold La Niña years. This result suggests that the amplitude of the seasonal cycle is affected by interannual variations in the depth of the thermocline and in the intensity of the trade winds.

1. Introduction

The Walker and Bliss (1932) pioneering studies of the Southern Oscillation fell into oblivion for several decades after their results were published. One reason was the failure of the authors to identify a physical mechanism that could explain the remarkable correlation between various meteorological variables as measured in the tropical Pacific and Indian Oceans over extended periods. The second reason for the neglect of Walker and Bliss' findings is more intriguing: the Southern Oscillation faded away after Walker and Bliss published their results! Troup (1965), who reanalyzed Walker's datasets after extending them to include more recent data, found that the Southern Oscillation was a more coherent signal during the period 1880–1920 studied by Walker than during the period 1920–1950. The correlation between sea level pressure at Darwin and Honolulu, for example, decreased from −0.66 to −0.12. Trenberth and Shea's (1987) analysis of sea level pressure anomalies at Darwin and other stations (after removal of the annual cycle) confirmed that the Southern Oscillation was very strong from 1900 to 1920 but did not become conspicuous again until after the late 1930s. Elliott and Angell (1988) also showed that 1920 signaled the start of a period of decreased interannual variability. In a recent study, Rasmusson (1993, personal communication) applied singular spectrum analyses to data that included sea level pressure at Bombay between 1847 and 1990, and SST of the region 0°–10°S and 90°W–180°. He found that the variance of the Southern Oscillation has changed by a factor of 2 or more during the past century. It was pronounced late in the nineteenth century relatively weak between 1920 and 1950 and has increased in intensity since then. Cole et al. (1992) analyzed the concentration of the isotope δO^{18} (which measures rainfall) in corals from Tarawa (1°N, 172°E) for the period 1895–1985. They divided the time series into three parts, each 30 years long, calculated a spectrum for each period, and showed how the amplitudes of the interannual variability and the annual cycle changed from period to period. Their results confirm earlier studies. For a discussion of secular changes in the amplitude and period of El Niño over much longer timescales (several centuries), the reader is referred to the articles in Diaz and Margraf (1992). The proxy data from tree rings (Michaelsen 1989) and floods of the Nile (Diaz and Pulwarty 1992; Anderson 1992), for example, suggest that in the past both the amplitude and the period of El Niño fluctuated significantly. The recurrence rate was stationary for the El Niño but significantly nonstationary for the strong El Niño at centenary timescales (Enfield and Cid 1991).

The Southern Oscillation is a natural mode of oscillation of the coupled ocean–atmosphere system. [See Philander (1990), Cane (1992), and Neelin et al. (1994) for reviews of this topic.] Stability analyses reveal that there is a broad spectrum of such modes and that the Southern Oscillation corresponds to one of the most unstable modes. The seasonal variations in solar

Corresponding author address: Dr. Daifang Gu, Program in Atmospheric and Oceanic Sciences, P.O. Box CN710, Sayre Hall, Princeton University, Princeton, NJ 08544-0710.

radiation also excite ocean–atmosphere modes (Chang and Philander 1994). There is convincing evidence, observationally and theoretically, that the annual and interannual mode interact, but the nature of the interaction is poorly understood. For example, it is not known why El Niño episodes between 1950 and 1980 started in the eastern equatorial Pacific during the warm phase of the seasonal cycle in the region (March and April) (Rasmusson and Carpenter 1982), whereas subsequent El Niño episodes start in the western equatorial Pacific during the fall equinox. Further evidence of interaction comes from efforts to predict El Niño by means of coupled ocean–atmosphere models; there is success only if the seasonal cycle is taken into account (Latif et al. 1994). Nonlinear interactions between the annual and interannual fluctuations have recently been identified as possible contributors toward the irregularity of the Southern Oscillation (Tziperman et al. 1994; Jin et al. 1994; Chang et al. 1994). If true, then those interactions control the predictability of El Niño.

Not only does the seasonal cycle influence El Niño, but the converse is also true. Ramage (1975), for example, has established that the seasonal migrations of the intertropical convergence zone are inhibited during El Niño. We hope to shed light on the poorly understood relations between the interannual variability and the seasonal cycle by studying the concurrent secular fluctuations of the variability on these two timescales.

This paper is an analysis of the Comprehensive Ocean–Atmosphere Data Set (COADS) for the purpose of investigating secular changes in the amplitudes of interannual variability and the seasonal cycle in the Tropics. Usually, the seasonal cycle is defined as the climatological monthly mean of the data, and the interannual variability is the departure from that mean. With such a definition the seasonal cycle has no year-to-year variation. For our purposes the seasonal cycle and the interannual variability have to be separated in a different manner. We propose to use the recently developed wavelet transform method. In conventional Fourier analyses, a time series is mapped onto frequency space in such a manner that all information about the time domain is lost. In the wavelet method, a time series is mapped onto both frequency and time space, so that it is possible to see how the amplitude of fluctuations at a particular frequency varies with time. This method has been applied to many fields of science and engineering, but its application is relatively novel in meteorology and oceanography. This paper, therefore, includes a brief discussion of the method.

The organization of this paper is follows. Section 2 concerns wavelet transforms that are relevant to this research, and section 3 describes the data to be used. Section 4 and section 5 illustrate the decadal variations of ENSO (El Niño/Southern Oscillation) and the annual cycle. Section 6 discusses the factors that influence decadal variation, and section 7, the influence of ENSO on the annual cycle. Section 8 summarizes the results.

2. Data analysis method: Wavelet transforms

ENSO and the seasonal cycle are well separated in frequency space: ENSO covers the frequency range from 0.2 to 0.5 cycles per year, while the seasonal cycle has sharp peaks at frequencies of 1.0 and 2.0 cycles per year. Figure 1 shows a typical SST spectrum for the equatorial region. It provides no information about the manner in which the amplitude of fluctuations at a specific frequency varies with time. Such information becomes available when wavelet transforms rather than Fourier transforms are used. For a detailed description of this method the reader is referred to the book by Combes et al. (1989), and the reviews by Farge (1992) and Meyers et al. (1993). Here we briefly summarize the main points.

Let $f(t)$ be a signal that varies with time. Its wavelet transform is then defined as follows:

$$\tilde{f}(t', a) = \frac{1}{a^{1/2}} \int f(t)\psi^*\left(\frac{t - t'}{a}\right)dt, \quad (2.1)$$

where $\tilde{f}(t', a)$ is the wavelet coefficient, t' is the translation parameter corresponding to the position of the wavelet, and a is the scale dilation parameter that determines the width of the wavelet. The function $\psi(t)$ is called the mother wavelet. It generates a family of wavelets by translation and dilation, and ψ^* is the complex conjugate of ψ. The wavelet coefficients can also be written in terms of Fourier transforms $\hat{f}(\omega)$, $\hat{\psi}(\omega)$ of $f(t)$, and $\psi(t)$:

$$\tilde{f}(t', a) = a^{1/2} \int \hat{f}(\omega)\hat{\psi}(a\omega)e^{-it'\omega}d\omega, \quad (2.1')$$

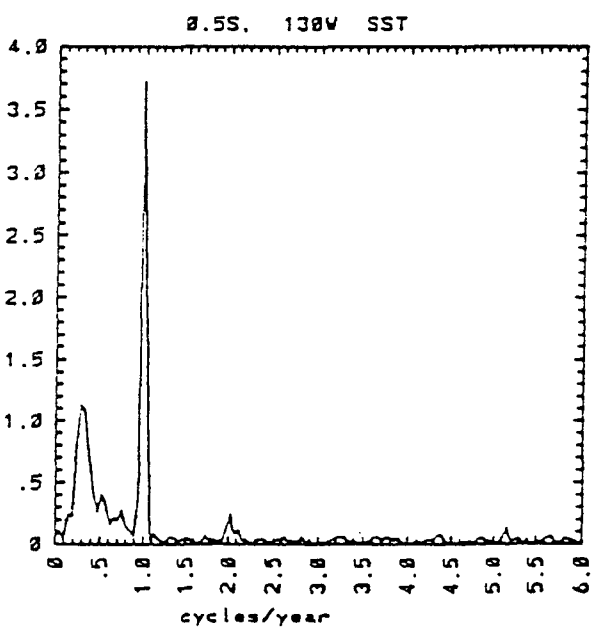

FIG. 1. Spectrum of SST at 0.5°S, 130°W. The scale on the vertical axis is arbitrary.

where the Fourier transform is defined as

$$\hat{\psi}(\omega) = \frac{1}{2\pi} \int \psi(t) e^{-il\omega} dt. \quad (2.2)$$

It follows that the scale decomposition is obtained by the translation and dilation of only one "mother" function. Thus, all the wavelets in a family generated by one "mother wavelet" are similar in that they are scale invariant with one another; in particular, they all have the same number of oscillations. In this respect they differ from a windowed Fourier transform, whose scale decomposition is based on a family of trigonometric functions with an increasing number of oscillations as the scale decreases because of the fixed width of the window.

The only constraint imposed on the mother wavelet $\psi(t)$ is the admissibility condition

$$C_\psi = 2\pi \int |\hat{\psi}(\omega)|^2 \frac{d\omega}{\omega} < \infty. \quad (2.3)$$

If $\psi(t)$ is integrable, the above admissibility implies that it has a zero mean

$$\int \psi(t) dt = 0 \quad \text{or} \quad \hat{\psi}(\omega = 0) = 0. \quad (2.4)$$

In practice the wavelets have limited spatial support in time space. The signal at infinity, therefore, does not influence the wavelet coefficients, and the wavelet analysis or synthesis can be performed locally.

The admissibility condition (2.3) ensures the recovery of the signal from its wavelet coefficients

$$f(t) = \frac{1}{C_\psi} \int_0^\infty \frac{da}{a^2} \int \tilde{f}(t', a) \psi\left(\frac{t - t'}{a}\right) dt'. \quad (2.5)$$

If $\psi(t)$ is complex valued and $f(t)$ real valued, then we should take only the real part of Eq. (2.5).

An important property of wavelet transforms is the conservation of energy:

$$\int_{-\infty}^{+\infty} |f(t)|^2 dt = \frac{1}{C_\psi} \int_{0+}^{+\infty} \frac{da}{a^2} \int_{-\infty}^{+\infty} |\tilde{f}(t', a)|^2 dt'. \quad (2.6)$$

Because of this conservation property, no information is lost in transforming the signal into wavelet coefficients. The conservation of energy is also valid locally if one considers all the wavelet coefficients inside the "influence cone," which is defined as a region in time space that supports all dilated wavelets.

The total energy can be split into different scales a:

$$E(a) = \frac{1}{C_\psi} \int_{-\infty}^{+\infty} |\tilde{f}(t', a)|^2 \frac{dt'}{a^2}, \quad (2.7)$$

where E is known as the wavelet spectrum.

Since the admissibility is the only condition that is required for an analyzing function $\psi(t)$ to be a mother wavelet, one can construct many different mother wavelets. When choosing a mother wavelet to analyze a signal, we must keep in mind that the wavelet transform is an inner product of the signal and the analyzing wavelet at scale a. The wavelet coefficients combine the information about both the signal and the wavelet. The appropriate mother wavelet, real or complex, is the one that can best extract the required information from the signal. A commonly used real-valued wavelet is the second derivative of the Gaussian, which is called a "Mexican hat." A commonly used complex-valued wavelet is the Morlet wavelet, which is a plane wave of frequency ω_ψ, modulated by a Gaussian envelope. The complex-valued wavelets are also called progressive wavelets. For this study, the complex-valued wavelets are appropriate because they allow us to depict amplitudes (or energy) and phase of the scale a as a function of time. The Morlet wavelet is particularly good for the annual cycle, which is approximately sinusoidal. ENSO is less periodic, but in a recent study by Rasmusson (1993, personal communication), the principal component of ENSO was found to be essentially sinusoidal. Therefore, the Morlet wavelet also provides a reasonably good representation of ENSO.

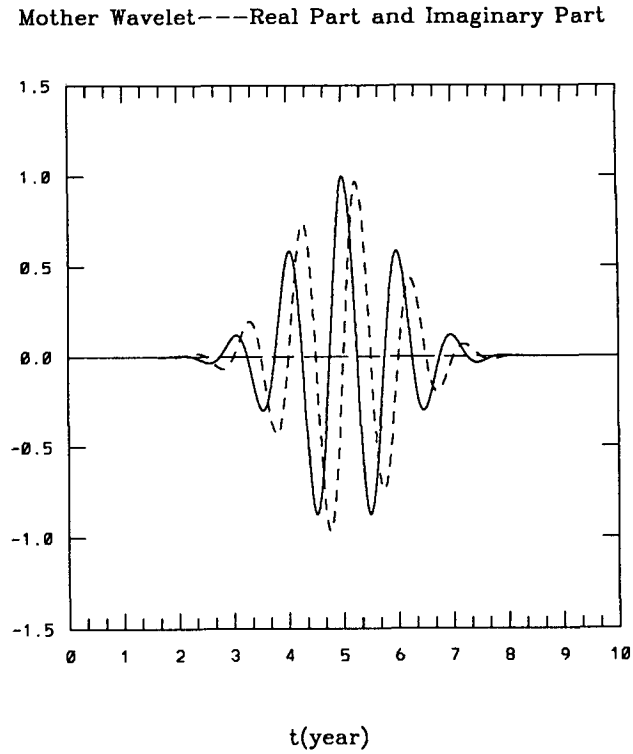

FIG. 2. Mother wavelet (Morlet) used in this paper. Solid line: real part of the mother wavelet. Dashed line: imaginary part of the mother wavelet.

The mother wavelet we use in this study has the form

$$\psi(t) = e^{-i2\pi t} \exp\left[-\left(\frac{2\pi}{k_\psi}\right)^2 |t|^2/2\right], \quad (2.8)$$

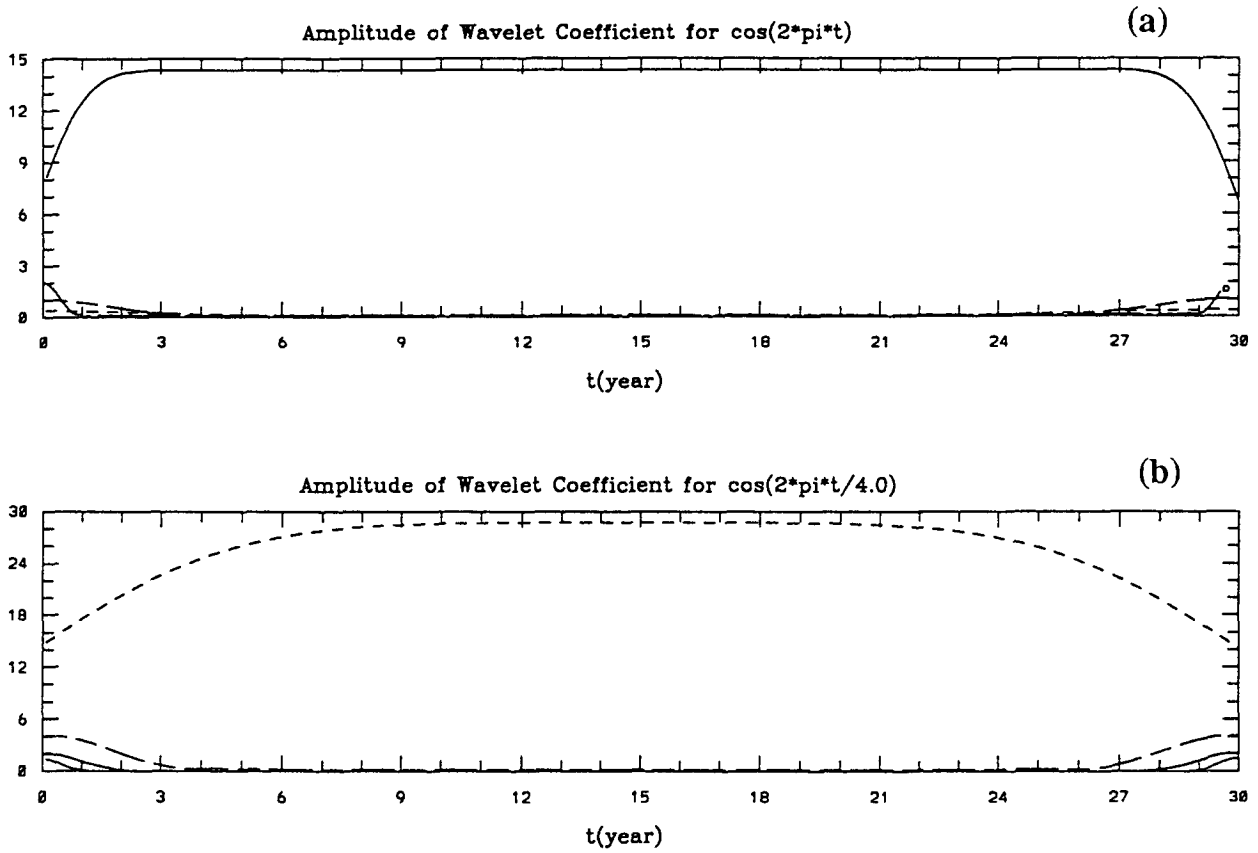

FIG. 3. Modulus of wavelet coefficients for $\cos(2*pi*t)$ and $\cos(2*pi*t/4)$ with $0 < t < 30$ (year). - - - O - - -: $a = 0.5$. Solid line: $a = 1$. Long-dashed line: $a = 2$. Short-dashed line: $a = 4$.

where t has unit of a year, and k_ψ is a constant that defines the width of the Gaussian envelope of the mother wavelet. The term k_ψ remains constant during wavelet transform calculations. The wavelet coefficient at scale $a = 1$ gives information about the annual cycle and that at scale $a = 0.5$ gives information about the semiannual cycle. The Morlet wavelet is admissible only for values of $|k_\psi|$ that are approximately equal to or larger than 6 (Farge 1992). As $|k_\psi|$ increases, the time resolution of the wavelet coefficients decreases, since the width of the Gaussian envelope increases. For the best time resolution, we should choose the smallest allowable value for $|k_\psi|$. In this study we choose it to be 6.

The shape of the mother wavelet, shown in Fig. 2, is such that its value is practically zero three years from the center of the mother wavelet. As an example, consider the signal

$$g(t) = \cos(2\pi t) \quad (0 < t < 30).$$

The modulus, or amplitudes, of the wavelet coefficients, defined as $|\tilde{f}(t', a)|$, are shown in Fig. 3 for $a = 0.5$, 1, 2, and 4. The amplitude of $a = 1$ is a straight line except at the beginning and the end of the dataset. The straight line indicates that the amplitude of the signal is constant at a frequency of one cycle per year. The distortion of the results usually occurs within regions $3*a$ from the beginning and end points. The amplitudes for $a = 0.5$, 2, and 4 are very small, and thus the energy leakage to other cycles, such as the semiannual, two-year, and four-year cycles, is very small. Results for the case $g(t) = \cos(2\pi t/4)$, which represents the four-year cycle shown in Fig. 3b, are similar. These examples demonstrate that the Morlet wavelet is an appropriate wavelet to deal with both ENSO and the annual cycle.

The next example demonstrates the difference between Fourier and wavelet spectra. Consider the signal

$$f(t) = \cos(2\pi t/8)\cos(2\pi t) \quad (0 < t < 30)$$

shown in Fig. 4a. The Fourier spectrum consists of two delta functions at frequencies of 0.875 and 1.125 cycles per year. It has no explicit information about the envelope of the carrying wave, which has a period of four years. Such information is readily available from the amplitude of the wavelet coefficient for $a = 1$ shown in Fig. 4b. It varies with a period of four years, while the amplitudes for $a = 0.5$, 2, and 4 are very small and can be neglected. Examples similar to this one will be encountered in sec-

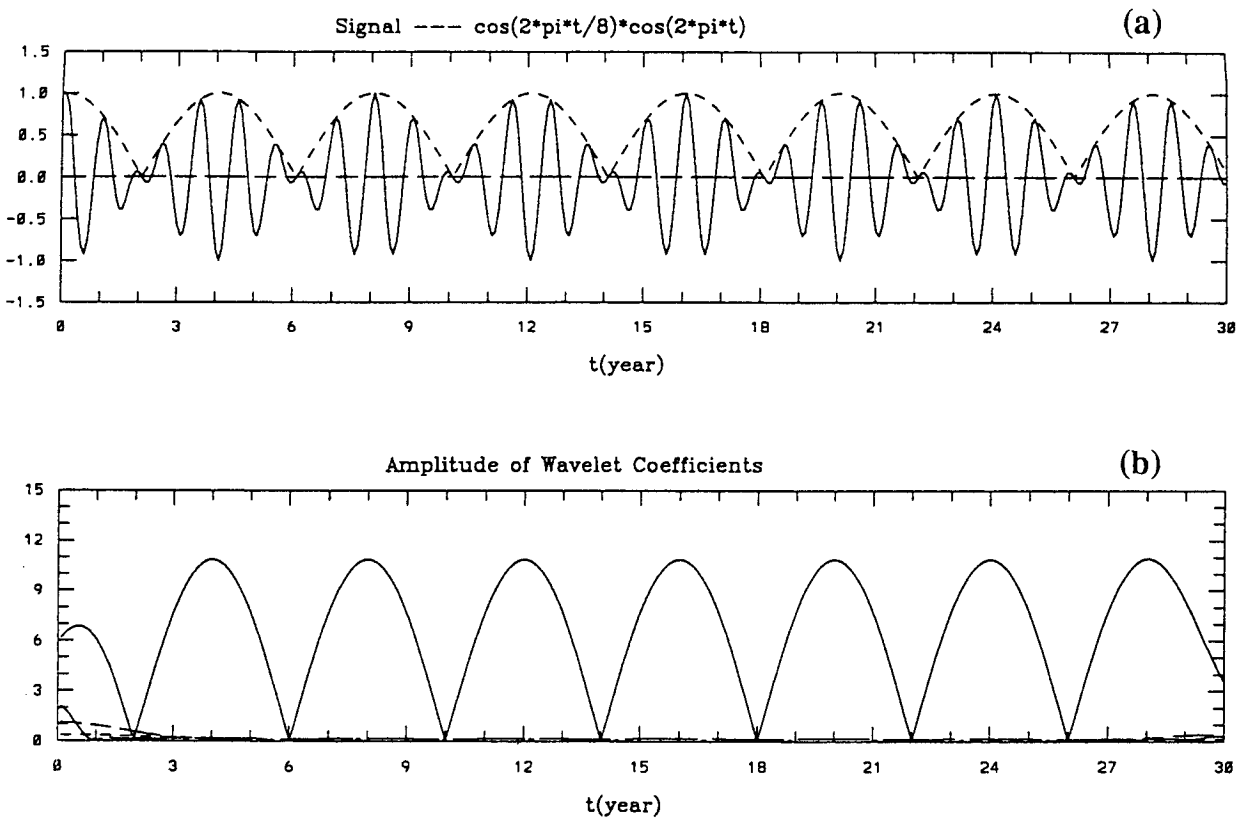

FIG. 4. Upper panel: signal of $\cos(2*pi*t/8)\cos(2*pi*t)$. Solid line: signal. Short-dashed line: envelope of the signal. Lower panel: modulus of wavelet coefficients. - - - O - - -: $a = 0.5$. Solid line: $a = 1$. Long-dashed line: $a = 2$. Short-dashed line: $a = 4$.

tions 4 and 5, which describe the amplitudes of the annual and interannual variability in the tropical Pacific.

3. Data

The data used in the present study are SST and zonal and meridional wind speeds (U, V) from COADS, with 1° lat by 1° long spatial resolution, prepared at the Geophysical Fluid Dynamics Laboratory for each month of the 119-year period from 1870 to 1988 (Pan and Oort 1990). The available observations before 1950 are quite sparse in the tropical Pacific except in a few shipping lanes, but the observations in the tropical regions of the Atlantic and the central and eastern Indian Oceans are much denser for the same period (Pan and Oort 1990). The spatial coverage of the observations and the number of observations in these three oceans increase greatly after 1950.

The longest available time series for the equator are from those points where the shipping lanes cross the equator. In the central and eastern Indian Ocean and in the central Atlantic Ocean, these points happen to be in regions where the SST signal has a significant amplitude, but that is not so in the Pacific, which has few shipping lanes. The problem can be mitigated by averaging the data over a large area. A check on this procedure is available for those regions that are intersected by a shipping lane. We find that, for the Pacific, COADS data averaged over an area of 20° long by 8° lat are reasonably accurate and are adequate for a study of interannual variability and the seasonal cycle. From COADS we generated time series for the following regions: 2°S–2°N, 63°–67°E, in the central Indian Ocean; 2°S–2°N, 28°–32°W in the central Atlantic Ocean; and 4°S–4°N, 170°E–170°W; 4°S–4°N, 140°–160°W; 4°S–4°N, 110°–130°W; and 4°S–4°N, 85°–105°W in the central and eastern Pacific Ocean. There have been significant changes in the techniques and instruments that are used to measure sea surface temperatures, especially in the late 1930s and early 1940s. Unfortunately, there is no consensus on how the data should be modified to take into account these changes. In this study, we follow Folland et al. (1984) and add 0.3°C to the data prior to April 1940, and 0.25°C to the data taken between April 1940 and December 1941. Our results are not sensitive to these corrections.

4. Secular variations of ENSO

A typical wavelet spectrum, obtained by using the mother wavelet of Eq. (2.8), is shown in Fig. 5. It has

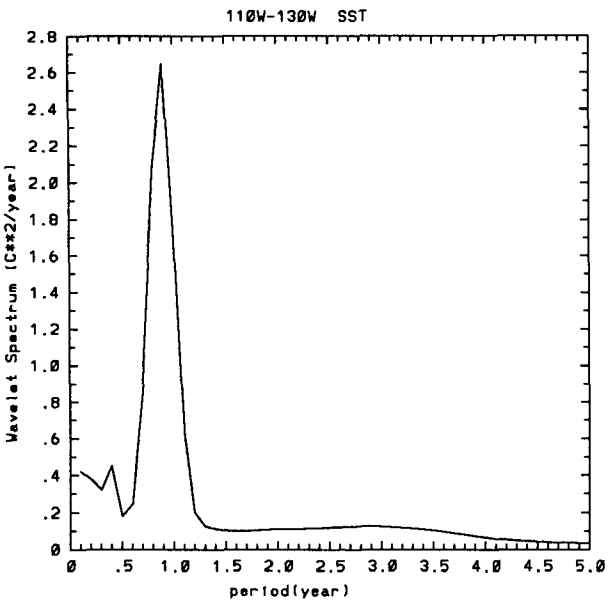

FIG. 5. Wavelet spectrum of SST at 0°N, 110°–130°W. The scale on the vertical axis is arbitrary.

minima around $a = 0.6$, which separates the annual cycle from the semiannual cycle, and around 1.7, which separates the annual cycle from interannual variability. Although the peak near 3.0 seems low, it represents a considerable amount of variance because the period of interannual variability ranges from 2 to 5 yr. The variance in the range of $0.7 \leqslant a \leqslant 1.2$ can be regarded as that of the annual cycle,

$$E_a(t') = \frac{1}{C_\psi} \int_{0.7}^{1.2} |\tilde{f}(t', a)|^2 \frac{da}{a^2}, \qquad (4.1)$$

and the variance in the range of $1.7 \leqslant a \leqslant 5.0$ is effectively that of the ENSO cycle,

$$E_i(t') = \frac{1}{C_\psi} \int_{1.7}^{5.0} |\tilde{f}(t', a)|^2 \frac{da}{a^2}, \qquad (4.2)$$

which includes the biennial variability. The amplitudes of the annual and ENSO cycles are therefore $[E_a(t')]^{1/2}$ and $[E_i(t')]^{1/2}$, respectively.

The wavelet method allows a description of changes in the amplitude of the Southern Oscillation but does not give detailed information about changes in frequency. Limited information is available from spectra such as that in Fig. 5. The broad, relatively flat shape of the spectrum at a period from 2 to 5 yr indicates the absence of a single dominant frequency over the past century.

The solid lines in Fig. 6 show the variation of E_i, the variance of ENSO cycles as measured by SST along the equator between 1885 and 1975; locations are indicated in each panel. Results for the periods 1870–1884 and 1976–1988 have been discarded because they fall in the influence cones of the end points of the original time series with respect to $a = 5$. Note that the vertical scale changes from panel to panel, a choice that emphasizes the variation rather than the absolute value of the variance in ENSO at each location. In Fig. 6, interannual variability in SST has its largest variance in the eastern tropical Pacific in the decades up to 1915 and after 1960. Amplitudes are generally small between 1915 and 1950. This is consistent with the results of earlier investigators mentioned in the introduction. When we turn to fluctuations in the zonal component of the wind, the dashed lines shown in Fig. 6, we find that the western Pacific up to the date line approximately has the largest variance. In general, when the wind fluctuations in the west are energetic, then sea surface temperature variations in the eastern tropical Pacific are large. This is consistent with previous analyses (see, for example, Chao and Philander 1993) and with models of ENSO.

Variations in the equatorial Indian and Atlantic Oceans, shown in Fig. 7, have a far smaller variance than those in the equatorial Pacific. The fluctuations in the Indian Ocean tend to resemble those in the Pacific, which may be an indication that ENSO, a phenomenon primarily of the Pacific, also has a signature in the Indian Ocean.

5. Secular variations of the annual cycle

The secular variations in the variance of the annual cycle of SST E_a are shown in Fig. 8 for the equatorial zones centered on 120°W in the eastern Pacific and 30°W in the Atlantic. It is evident that in the Pacific there are fluctuations on the short timescale of about 3–5 yr, that of ENSO, a matter to which we return in section 7. On the decadal timescale, there appears to be no relationship between the variance of the annual cycle and the variance of the ENSO cycles. Thus, between 1915 and 1950, when the variance of the ENSO cycle is relatively low, the variance levels of the annual cycle on the equator near 120°W are about the same as those in the preceding and subsequent decades when the variance of the ENSO cycle is relatively large. The same is true of the annual cycle in other equatorial regions, the western Pacific, and the Indian and the Atlantic Oceans, all of which have smaller variance for the annual cycle of SST than the eastern Pacific. We must keep in mind, however, that our analyses are of time series at selected locations along the equator and give no information about latitudinal structures. Because of a lack of data, we cannot exclude the possibility that variations in the spatial structure of the seasonal cycle accompany the secular variations of ENSO.

6. Factors that influence decadal variations

Pan and Oort (1990) refer to the neighborhood of 0°N, 130°W as a "key region" because the fluctuations

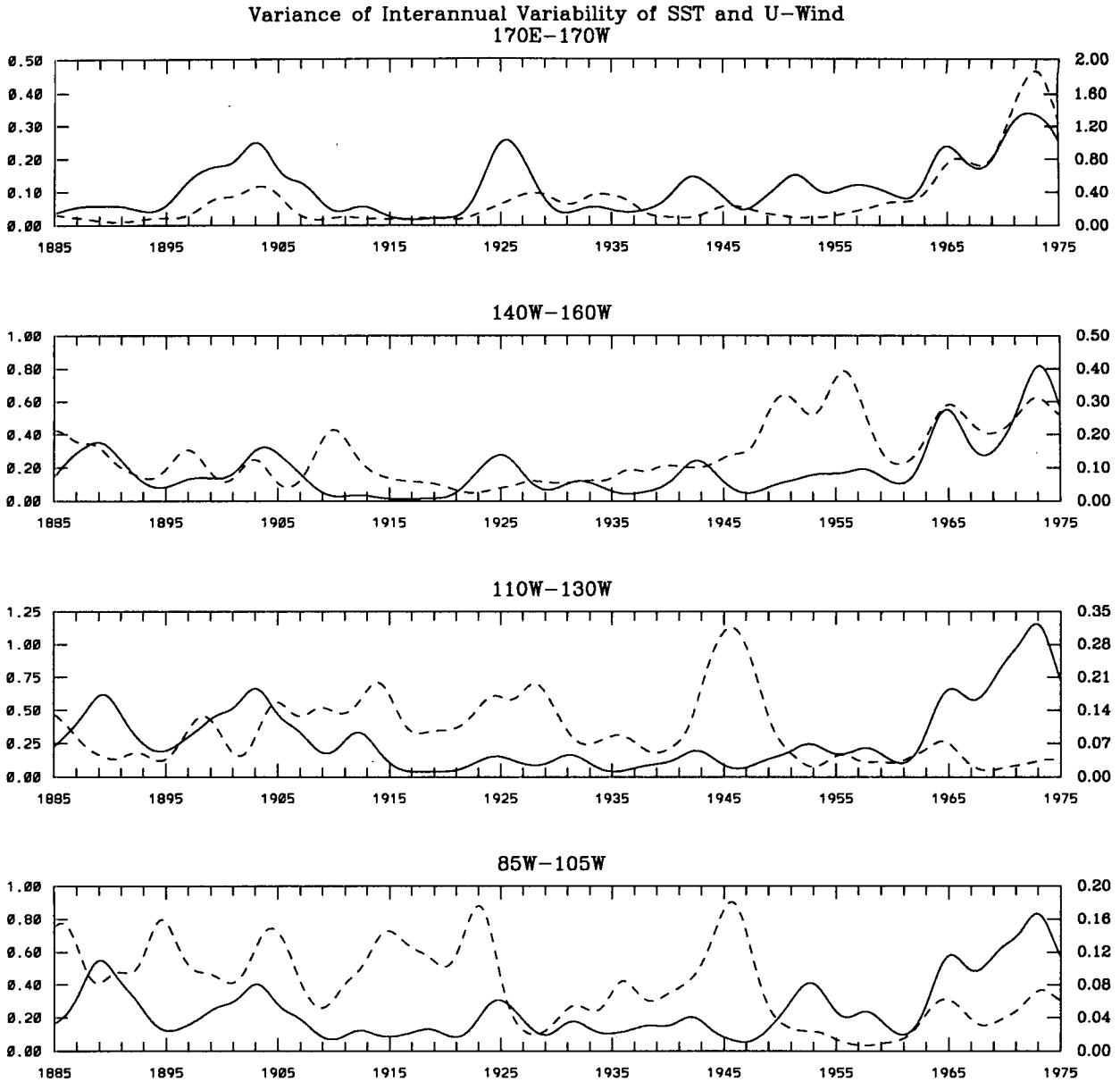

FIG. 6. Variance of interannual variability in the Pacific along the equator. Solid lines: SST. Dashed lines: zonal wind speed. The scales on the left vertical axes are for temperature in $(°C)^2$, and the scales on the right are for the wind speed in $(m\ s^{-1})^2$. The latitudinal span of the data: 4°S–4°N.

of sea surface temperatures in that region are correlated with the fluctuations of many meteorological parameters in different parts of the globe. Figure 9 shows the 161-month running mean of SST in this key region (2°S–2°N, 123°–127°W). This filter retains decadal fluctuations while eliminating variations with a shorter timescale. The choice of 161 months is somewhat arbitrary; an 81-month running mean gives practically the same results. From a comparison of Figs. 6 and 9, it is evident that there is essentially no correlation between the energy of the ENSO cycle and decadal variations of SST at 0°, 125°W. [The various correlation coefficients range from 0.3 to 0.4, and none of them exceeds the 70% significant level by one tail t test assuming three degrees of freedom (Spiegel 1992).]

Since 1970 there has been a discernible increase in globally averaged air temperatures. Is that correlated with the large increase in the amplitudes of ENSO during the same period? Comparison of the curves in Fig. 6 with the annual mean surface air temperature in the Northern Hemisphere and Southern Hemisphere (Peixoto and Oort 1992, Fig. 16.18) again shows no

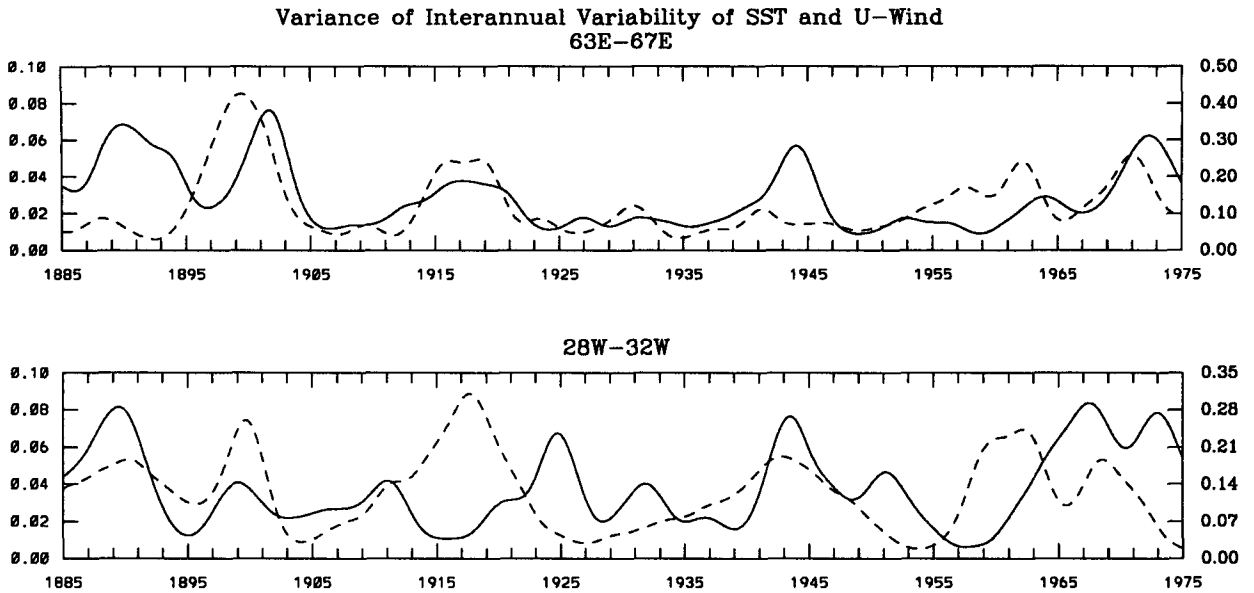

FIG. 7. Same as in Fig. 6 but in the Indian and Atlantic Oceans. The latitudinal span of the data: 2°S–2°N.

correlation. For example, air temperature rose in both hemispheres after 1960, a period during which ENSO had a relatively large variance; however, air temperature also rose in both hemispheres during 1920–1940, a period during which ENSO had a relatively small variance. The relevant correlation coefficients range from 0.05 to 0.32, and none of them exceeds the 60% significant threshold. Further research is therefore needed to understand the decadal variations in ENSO.

7. Influence of ENSO on the annual cycle

The amplitude (rms of the variance) of the annual cycle varies much more on interannual than decadal timescales. (See Fig. 8.) In Fig. 10 this amplitude of SST (solid line) is superimposed on the interannual variation of SST (dashed line) at 2°S–2°N, 123°–127°W; 2°S–2°N, 101°–105°W; and 2°S–2°N, 88°–92°W. The dashed line, obtained using 15-point

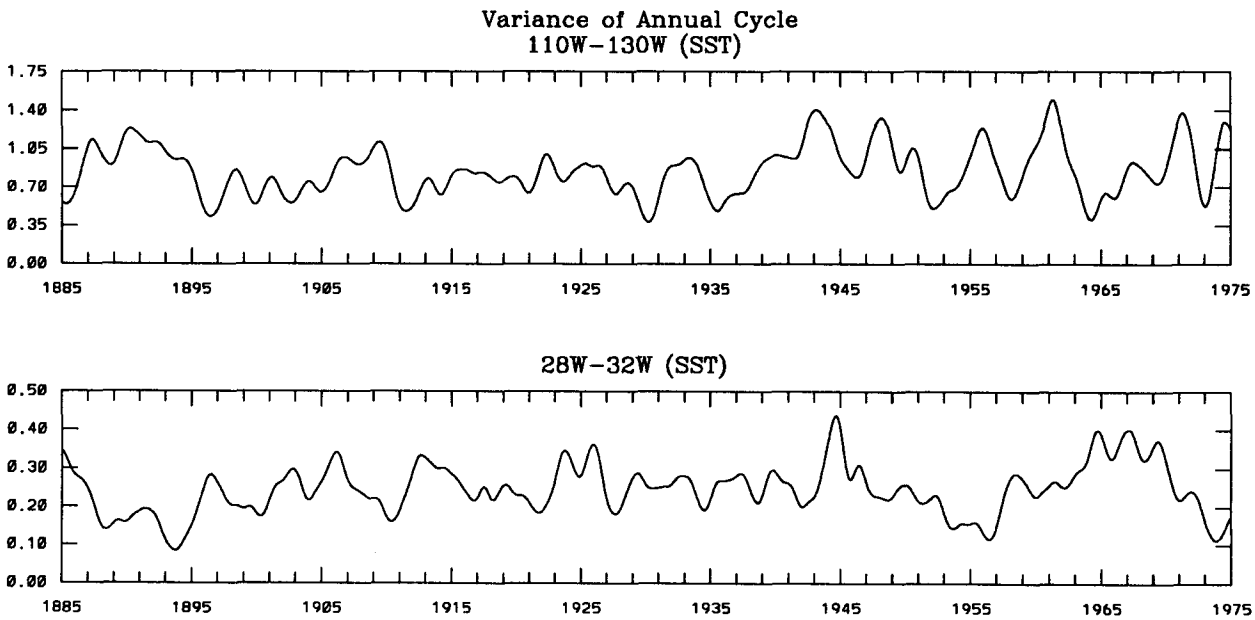

FIG. 8. Variance of annual cycle of SST in the Pacific and Atlantic along the equator. The unit on the vertical axis is $(°C)^2$.

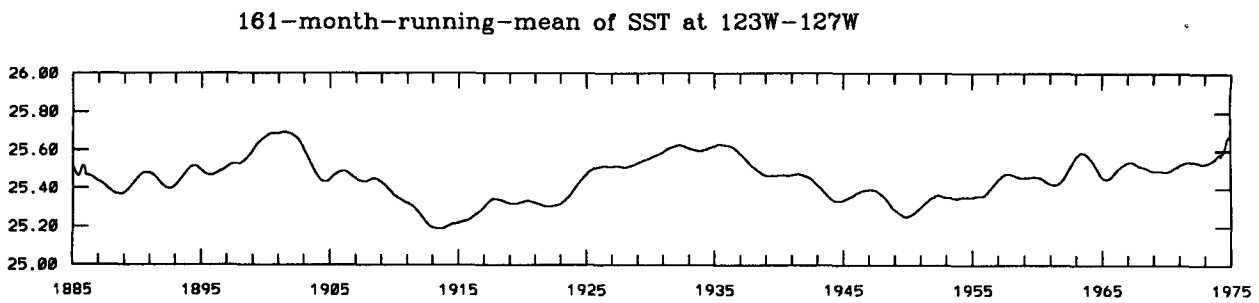

FIG. 9. 161-month running mean of SST at 2°S–2°N, 123°–127°W. The unit on the vertical axis is degrees Celsius.

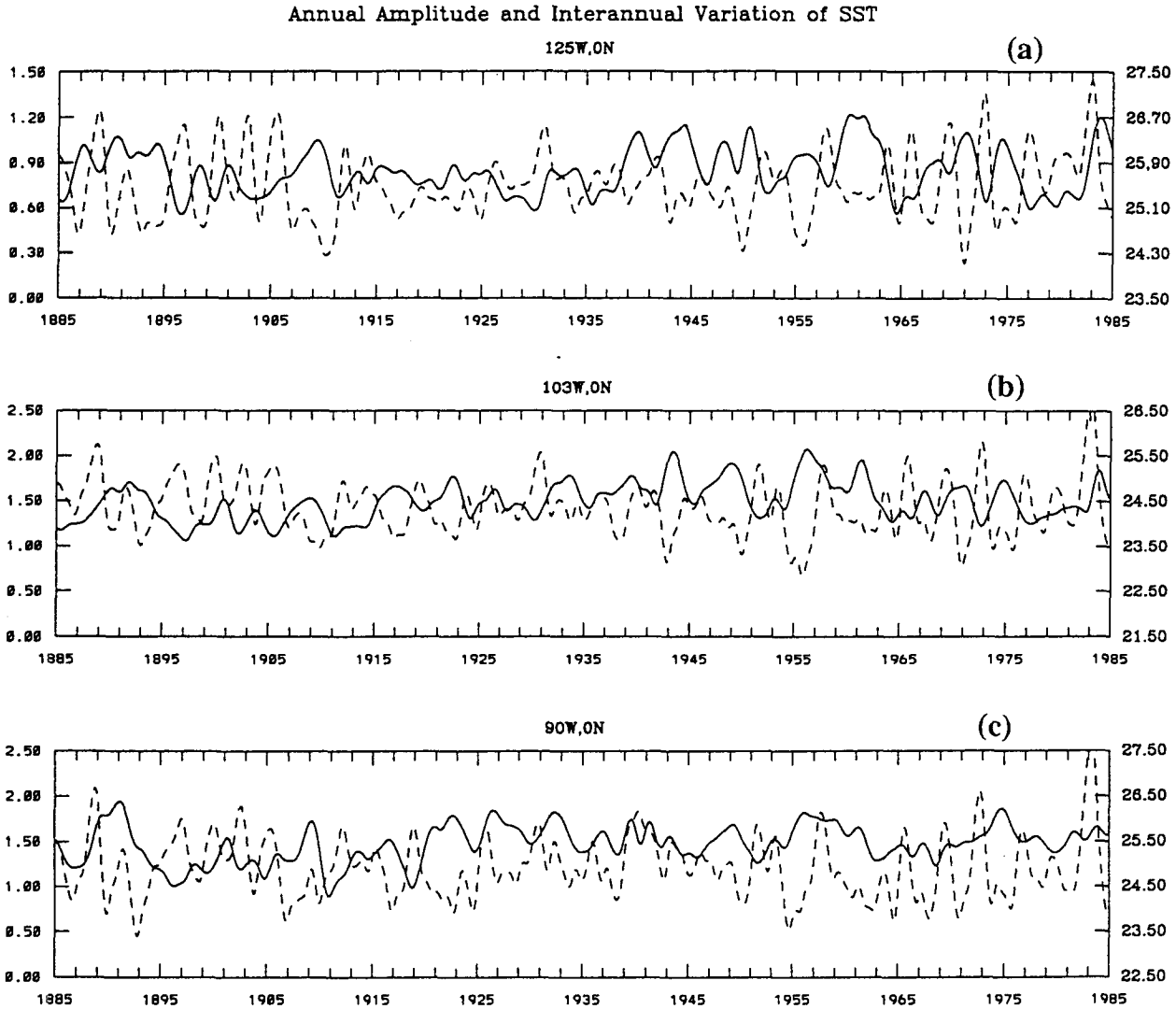

FIG. 10. Solid line: Amplitude of annual cycle. Dashed line: interannual variation of SST obtained using a 15-point Gaussian-type filter. The scales on the left vertical axes correspond to the solid line with unit degrees Celsius, and the scales on the right correspond to the dashed line with unit degrees Celsius.

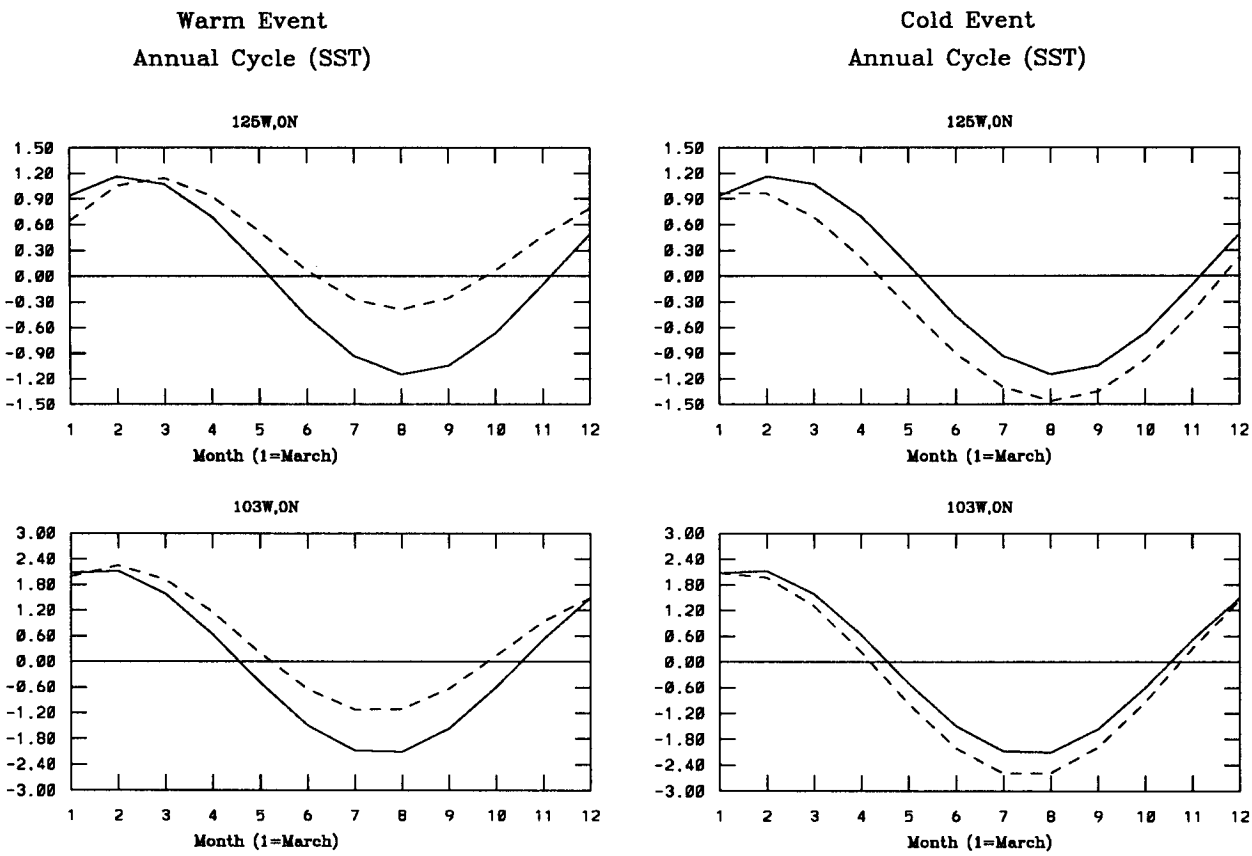

FIG. 11. Composite of the annual cycle of SST during 1950–1988. Solid line: composite of the mean annual cycle. Dashed line in the left two panels: composite of the annual cycle in warm years. Dashed line in the right two panels: composite of the annual cycle in cold years. The unit on vertical axes is degrees Celsius.

Gaussian-type filter, highlights warm El Niño and cold La Niña episodes. The correlation between the solid and dashed lines in Figs. 10a,b are −0.42 and −0.46, respectively. Both exceed the 99% significant threshold of a one-tail t test with 30 and 25 degrees of freedom for the two cases, respectively (Spiegel 1992). The correlation for the lines in Fig. 10c is only −0.10 and is statistically insignificant. Hence, the amplitude of the annual cycle is negatively correlated with the interannual variations of the local SST at 125° and 103°W along the equator. From a close inspection of Fig. 10, it is evident that the annual cycle becomes weaker during El Niño and stronger during La Niña.

For the period 1950–1988, data are sufficient to calculate the correlation between the interannual variation of local SST and the variance of the annual cycle for SST and zonal and meridional wind speeds over a large part of the eastern tropical Pacific. In general the correlation is high if the variables are sea surface temperatures, but the correlation is low if one variable is either wind component. Whereas the variations are slow and smooth in the case of SST, they are rapid and large in the case of the wind.

To understand the high negative correlation between the amplitude of the annual cycle of SST and the interannual variability of local SST, it is necessary to keep in mind that different physical processes determine sea surface temperature changes on seasonal and interannual timescales. Interannual changes are associated with a large-scale horizontal redistribution of warm surface waters: during El Niño the thermocline deepens in the eastern tropical Pacific while it shoals in the west. Seasonally there is practically no local change in the depth of the thermocline in those regions where seasonal sea surface temperature changes are large (Chang 1994; Koeberle and Philander 1994). The large seasonal SST changes in the eastern tropical Pacific are primarily due to the processes in the following equation:

$$\frac{\partial T'}{\partial t} = -\frac{1}{C_p\bar{H}} w' \frac{\partial \bar{T}}{\partial z} - \frac{1}{C_p\bar{H}} \bar{w} \frac{\partial T'}{\partial z} + Q' \quad (5.1)$$

with the horizontal advection being neglected as indicated by the measurements of Hayes et al. (1991). The barred quantities in (5.1) are defined as

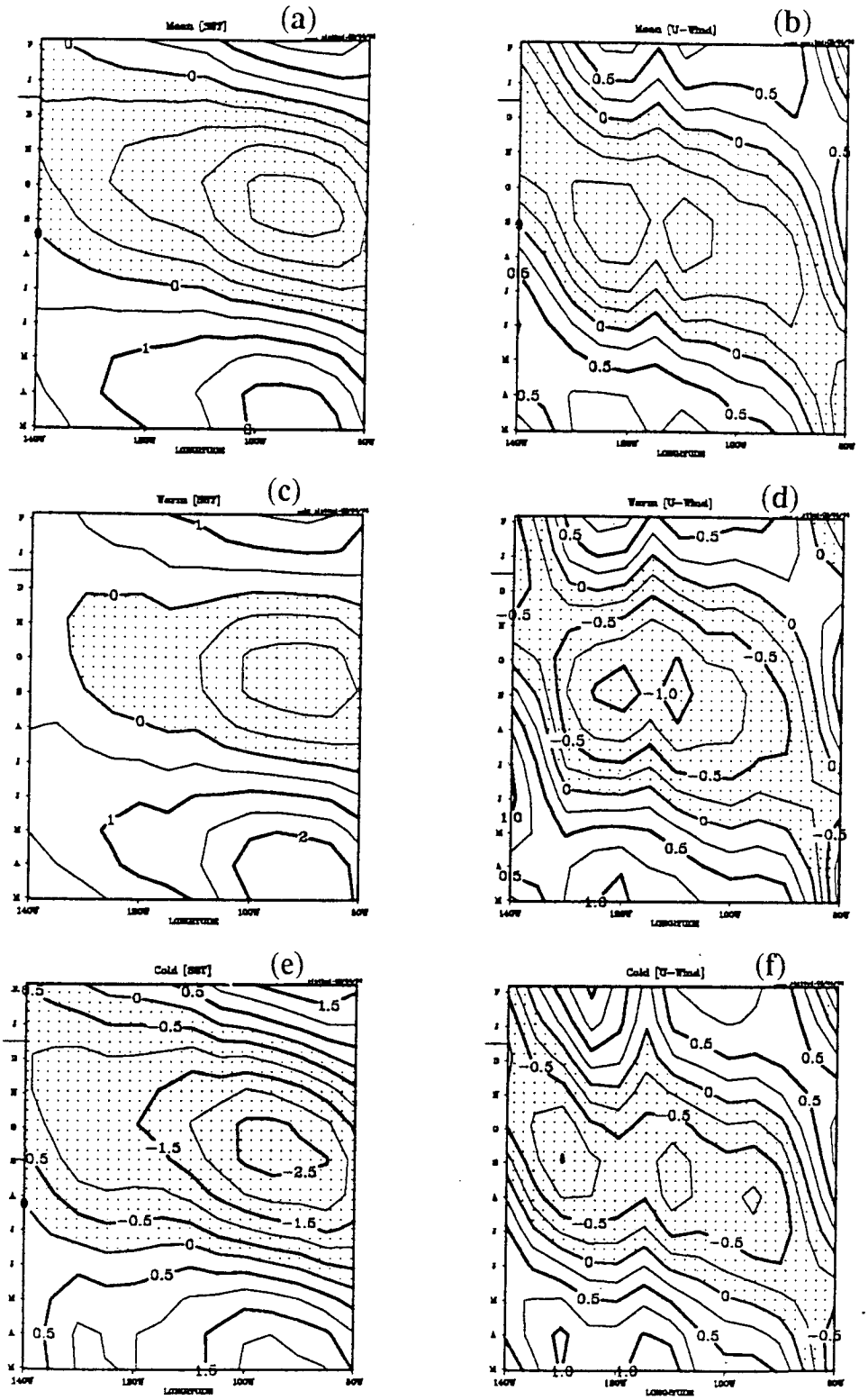

FIG. 12. Longitude–time plots of composite of the annual cycle along the equator. Time starts with March at the bottom and increases to February at the top. Longitudinal span is from 140° to 80°W. Dotted areas are the negative deviation from the annual mean. The contour intervals are 0.5°C for SST and 0.25 m s^{-1} for zonal wind. (a) Mean annual cycle of SST. (b) Mean annual cycle of zonal wind speed. (c) Annual cycle of SST during warm years. (d) Annual cycle of zonal wind speed during warm years. (e) Annual cycle of SST during cold years. (f) Annual cycle of zonal wind during cold years.

$$\bar{A}(t) = \frac{1}{2T_0}\int_{-T_0}^{T_0} A(t+t_1)dt_1 \qquad (5.2)$$

with $T_0 = 6$ months and can therefore be regarded as the interannual variability because variability with timescales shorter than 1 year has been filtered out. Thus, primed quantities A' can be regarded as the seasonal variability. The T is SST, w the vertical velocity, H the thermocline depth, and Q the net heat flux across the sea surface.

Since the upwelling velocity w is zero at the sea surface, the effects of upwelling on SST depend on the strength of mixing, which is determined by the intensity of the wind and by the stratification in the upper ocean. The net heat flux across the ocean affects the stratification and therefore affects the strength of mixing. For a larger heat flux, the upper layer becomes more stable and less stirred so that the SST increases.

In the southeastern equatorial Pacific, the meridional winds, which are generally northward, are weakest during March and April and strongest during August and September. The zonal winds, which generally are westward west of 90°W, have a much smaller seasonal variation (Horel 1982). Both the westward and northward winds induce equatorial upwelling and, hence, low sea surface temperatures in the southeastern equatorial Pacific (Philander and Pacanowski 1981). The relaxation of the meridional wind during March and April, and the large heat flux across the sea surface at that time contribute to the seasonal maximum in SST. During August and September, the strong upwelling due to stronger wind, together with a weak heat flux, produce a seasonal minimum in SST (Koeberle and Philander 1993).

Figure 11 contrasts the climatological annual cycle (solid line) with the annual cycle of El Niño (on the left) and La Niña (on the right) episodes on the equator at 125°W. (These composites are calculated from COADS data from 1950 to 1989.) The amplitude of the annual cycle is seen to decrease during the warm years and to increase during the cold years. This is consistent with the results obtained from the wavelet analyses in Figs. 10a,b. In Fig. 11 the differences between the solid and dashed curves are minimal in March and April of El Niño years. This is so because, during El Niño, the thermocline deepens in the eastern Pacific and the trades collapse so that $\bar{H}$ increases and $\bar{w}$ decreases. These changes have little effect during the northern spring when the mixing and upwelling are already at their seasonal minima. Their effect is large during the northern fall. In cold La Niña years the thermocline is shallower and the trades are stronger than normal; therefore, $\bar{H}$ is smaller and $\bar{w}$ is larger than normal. This means that, compared with the normal year, there is more upward flux of cold water throughout the year. Hence, SST of the annual cycle during a cold episode should be colder than normal throughout the cycle. Figure 11 shows that is the case.

In the eastern Pacific the seasonal cycle is characterized by westward phase propagation along the equator (Horel 1982; Philander and Chao 1991). This is a property of certain ocean–atmosphere interactions: a warm water anomaly induces a westerly wind anomaly to the west of the warm water; this westerly wind leads to higher SST to the west of the original anomaly so that the pattern moves westward (Neelin 1991). In warm years the thermocline in the eastern Pacific deepens. This weakens the coupling between the ocean and the atmosphere so that the westward phase propagation should be less pronounced during El Niño. This is indeed the case as shown in Fig. 12, which depicts the mean annual cycle and the annual cycle for warm and cold years along the equator.

8. Discussion and summary

This paper applies wavelet transform methods to the 119-year COADS dataset to study decadal variations in the amplitude of the Southern Oscillation and the annual cycle. The results indicate that the intensity of ENSO was relatively large late in the last century and early this century, was relatively small between 1915 and 1950, and increased rapidly again after 1960. Note that it is meaningless to speak of the amplitude of ENSO in a specific year such as 1960 because an ENSO cycle lasts 2–5 years. The time resolution of the wavelet transform appropriate for ENSO is about 5–10 years.

Surprisingly, the decadal variations in the amplitude of ENSO are not matched by corresponding variations in the amplitude of the annual cycle. However, large changes in the depth of the thermocline, such as the deepening during El Niño and the shoaling during La Niña, do affect the annual cycle in the eastern tropical Pacific significantly: the annual cycle has a smaller amplitude during El Niño than during La Niña. These changes in the annual cycle have a simple explanation, but the decadal variations in ENSO are a mystery.

Acknowledgments. We are in debt to Dr. Oort for many constructive suggestions on analyzing COADS datasets. We would like to thank Drs. K. Bryan, N.-G. Lau, Z. Liu, S. Manabe, M. McPhaden, E. Rasmusson, X. Wang, and S.-P. Xie for the helpful discussions and suggestions. This research had the support of GFDL/NOAA and NOAA under Grant NA26GP0057. The views expressed herein are those of the authors and do not necessarily reflect the views of NOAA or any of its subagencies.

REFERENCES

Anderson, R. Y., 1992: Long-term changes in the frequency occurrence of El Niño events. *El Niño—Historical and Paleoclimatic Aspects of the Southern Oscillation,* H. F. Diaz and V. Margraf, Eds., Cambridge University Press, 193–200.

Cane, M., 1992: Tropical Pacific ENSO models: ENSO as a mode of the coupled system. *Climate System Modeling,* K. Trenberth, Ed., Cambridge University Press, 583–614.

Chang, P., 1994: A study of seasonal cycle of sea surface temperature in the tropical Pacific Ocean using reduced gravity model. *J. Geophys. Res.*, **99,** 7725–7735.

——, and S. G. H. Philander, 1994: A coupled ocean–atmosphere instability of relevance to the seasonal cycle. *J. Atmos. Sci.*, **24,** 3627–3648.

——, B. Wang, T. Li, and L. Ji, 1994: Interactions between the seasonal cycle and the Southern Oscillation—Frequency entrainment and chaos in a coupled ocean–atmosphere model. *Nature,* submitted.

Chao, Y., and S. G. H. Philander, 1993: On the structure of the Southern Oscillation. *J. Climate,* **6,** 450–469.

Cole, J. E., R. G. Fairbanks, and G. T. Shen, 1992: Retrospective monitoring of the tropical ocean–atmosphere using chemical records from long-lived corals. *Proc. NRC/NAS Workshop on Decadal-Century Scale Climate Variability,* Irvine, CA.

Combes, J. M., A. Grossmann, and P. Tchamitchian, Eds., 1989: *Wavelets: Time-Frequency Methods and Phase Space.* Springer-Verlag, 315 pp.

Diaz, H. F., and V. Margraf, Eds., 1992: *El Niño—Historical and Paleoclimatic Aspects of the Southern Oscillation.* Cambridge University Press, 476 pp.

——, and R. S. Pulwarty, 1992: A comparison of Southern Oscillation and El Niño signal in tropics. *El Niño—Historical and Paleoclimatic Aspects of the Southern Oscillation.* H. F. Diaz, and V. Margraf, Eds., Cambridge University Press, 175–192.

Elliott, W. P., and J. K. Angell, 1988: Evidence for changes in Southern Oscillation relationships during the last 100 years. *J. Climate,* **1,** 729–737.

Enfield, D., and L. Cid, 1991: Low-frequency changes in El Niño–Southern Oscillation. *J. Climate,* **4,** 1137–1146.

Farge, M., 1992: Wavelet transforms and their applications to turbulence. *Ann. Rev. Fluid Mech.,* **24,** 395–457.

Folland, C. K., D. E. Parker, and F. E. Kates, 1984: Worldwide temperature fluctuations, 1856–1981. *Nature,* **310,** 670–673.

Hayes, S. P., P. Chang, and M. J. McPhaden, 1991: Variability of the sea surface temperature in the eastern equatorial Pacific during 1986–1988. *J. Geophys. Res.*, **96,** 10 553–10 566.

Horel, J. D., 1982: The annual cycle in the tropical Pacific atmosphere and ocean. *Mon. Wea. Rev.*, **110,** 1863–1878.

Jin, F. F., D. Neelin, and M. Ghil, 1994: El Niño on the Devil's staircase: Annual subharmonic steps to chaos. *Science,* **264,** 70–72.

Koeberle, C., and S. G. H. Philander, 1994: On the processes that control seasonal variations of sea surface temperatures in the tropical Pacific Ocean. *Tellus,* **46A,** 481–496.

Latif, M., T. P. Barnett, M. A. Cane, M. A. Flugel, and N. E. Graham, 1994: A review of ENSO prediction studies. *Climate Dyn.,* **9,** 167–179.

Meyers, S. D., B. G. Kelly, and J. J. O'Brien, 1993: An introduction to wavelet analysis in oceanography and meteorology: With application to dispersion of Yanai waves. *Mon. Wea. Rev.,* **121,** 2858–2866.

Michaelsen, J., 1989: Long-period fluctuation in El Niño amplitude and frequency reconstructed from tree-rings. *Aspects of Climate Variability in the Pacific and Western Americas. Geophys. Monogr.,* No. 55, Amer. Geophys. Union, 69–74.

Neelin, J. D., 1991: The slow sea surface temperature mode and the fast-wave limit: Analytic theory for tropical interannual oscillations and experiments in a hybrid coupled model. *J. Atmos. Sci.*, **48,** 584–606.

——, M. Latif, and F.-F. Jin, 1994: Dynamics of coupled ocean–atmosphere models: The tropical problem. *Ann. Rev. Fluid Mech.*, **26,** 617–659.

Pan, Y. H., and A. H. Oort, 1990: Correlation analyses between sea surface temperature anomalies in the eastern equatorial Pacific and the World Ocean. *Climate Dyn.*, **4,** 191–205.

Peixoto, J. P., and A. H. Oort, 1992: *Physics of Climate.* Amer. Inst. Phys., 520 pp.

Philander, S. G. H., 1990: *El Niño, La Niña and the Southern Oscillation.* Academic Press, London, 289 pp.

——, and R. C. Pacanowski, 1981: The oceanic response to cross-equatorial winds (with application to coastal upwelling in low latitudes). *Tellus,* **33,** 201–210.

——, and Y. Chao, 1991: On the contrast between the seasonal cycles of the equatorial Atlantic and Pacific Oceans. *J. Phys. Oceanogr.,* **21,** 1399–1406.

Ramage, C. S., 1975: Preliminary discussion of the meteorology of the 1972–73 El Niño. *Bull. Amer. Meteor. Soc.,* **56,** 234–242.

Rasmusson, E. M., and T. H. Carpenter, 1982: Variations in tropical sea surface temperature and surface wind fields associated with the Southern Oscillation/El Niño. *Mon. Wea. Rev.,* **110,** 354–384.

Spiegel, M. R., 1992: *Statistics.* 2d ed. Schaum's Outline Series, McGraw-Hill, Inc., 504 pp.

Trenberth, K. E., and D. J. Shea, 1987: On the evolution of the Southern Oscillation. *Mon. Wea. Rev.*, **115,** 3078–3096.

Troup, A. J., 1965: The "Southern Oscillation." *Quart. J. Roy. Meteor. Soc.*, **91,** 490–506.

Tziperman, E., L. Stone, M. Cane, and H. Jarosh, 1994: El Niño chaos: Overlapping of resonances between the seasonal cycle and the Pacific ocean–atmosphere oscillator. *Science,* **264,** 72–74.

Walker, G. T., and E. B. Bliss, 1932: World Weath. *V. Mem. Roy. Meteor. Soc.,* **4,** 53–84.